Fluorescent optical tomography with large data sets

George Y. Panasyuk,[1] Zheng-Min Wang,[1] John C. Schotland,[1] and Vadim A. Markel[1,2,*]

[1]Department of Bioengineering, University of Pennsylvania, Philadelphia, Pennsylvania 19104, USA
[2]Department of Radiology, University of Pennsylvania, Philadelphia, Pennsylvania 19104, USA
*Corresponding author: vmarkel@mail.med.upenn.edu

Received April 3, 2008; revised June 25, 2008; accepted June 30, 2008;
posted July 9, 2008 (Doc. ID 94630); published July 30, 2008

In recent years, optical tomography (OT) of highly scattering biological samples has increasingly relied on noncontact CCD-based imaging devices that can record extremely large data sets, with up to 10^9 independent measurements per sample. Reconstruction of such data sets requires fast algorithms. The latter have been developed and applied experimentally in our previous work to imaging of the intrinsic absorption coefficient of highly scattering media. However, it is widely recognized that the use of fluorescent contrast agents in OT has the potential to significantly enhance the technique. We show that the algorithms previously developed by us can be modified to reconstruct the concentration of fluorescent contrast agents.

OCIS codes: 110.0113, 170.3880.

Optical tomography (OT) is a biomedical imaging modality that utilizes nonionizing near-infrared light to probe tissue structure and function [1,2]. It allows quantitative reconstruction of a three-dimensional map of absorption and scattering coefficients of tissue samples as thick as ~10 cm with subcentimeter resolution [3,4]. One of the most promising applications of OT is the detection and localization of small tumors in soft tissues, for example, in breast imaging. It is generally recognized that the use of fluorescent contrast agents has the potential to significantly enhance this technique [5–8]. Thus, a subfield of OT has emerged in which one seeks to reconstruct the spatial map of the concentration of fluorescent molecules. We will refer to this modality as fluorescent optical tomography (FOT). FOT has been recently used *in vivo* to image breast cancer in humans, with very promising results [8].

Both FOT and nonfluorescent OT depend on numerical inversion of data, which is a very ill-posed problem [1]. The ill-posedness adversely affects the quality and spatial resolution of images. We have demonstrated theoretically [9], in simulations [10], and experimentally [3] that this problem can be partially alleviated by utilizing very large data sets that have recently became available with CCD-based noncontact imagers. By large data sets we mean here $\gtrsim 10^7$ independent measurements. It is logical to assume that FOT would also benefit from the use of large data sets. However, image reconstruction with large data sets requires specialized algorithms. In this Letter, we apply for the first time, to the best of our knowledge, the fast image reconstruction methods to FOT imaging.

In the experiments reported here the medium to be imaged is illuminated by a cw laser beam whose central wavelength is $\lambda_e = 775$ nm. We have used as the contrast agent indocyanine green (ICG), whose emission wavelength is $\lambda_f \approx 830$ nm. The propagation of light is modeled by the diffusion approximation to the radiative transport equation with the use of a number of additional approximations described below. Within the accuracy of these approximations, the densities of electromagnetic energy at the excitation and the fluorescent wavelengths, $u_e(\mathbf{r})$ and $u_f(\mathbf{r})$, obey a system of two coupled time-independent diffusion equations [11]:

$$-D\nabla^2 u_e(\mathbf{r}) + \alpha u_e(\mathbf{r}) = S(\mathbf{r}), \tag{1}$$

$$-D\nabla^2 u_f(\mathbf{r}) + \alpha u_f(\mathbf{r}) = \eta c \sigma_e n(\mathbf{r}) u_e(\mathbf{r}). \tag{2}$$

Here D and α are the intrinsic diffusion and absorption coefficients of the medium that are related to the parameters of the radiative transport theory μ_a (the absorption coefficient), μ_s (the scattering coefficient), and g (the scattering asymmetry parameter) by $D = c/3(\mu_a + \mu_s')$, $\alpha = c\mu_a$, where $\mu_s' = (1-g)\mu_s$ is the reduced scattering coefficient and c is the average speed of light in the medium. In addition, $n(\mathbf{r})$ is the number density of the fluorescent molecules, σ is the absorption cross section of an isolated fluorescent molecule, and η is the quantum efficiency of the fluorescence. Finally, $S(\mathbf{r})$ is an appropriate source term that describes the radiation at the excitation wavelength. In deriving Eqs. (1) and (2) we have neglected the dependence of D and α on the wavelength and also assumed that $\alpha \gg a(\mathbf{r}) \equiv \eta c \sigma_e n(\mathbf{r})$. The latter assumption will allow us to linearize the inverse problem of FOT as shown below.

The diffusion equations (1) and (2) are supplemented by the mixed boundary condition $(u + l\hat{\mathbf{n}}\cdot\nabla u)|_{\mathbf{r}\in\partial V} = 0$, where l is the extrapolation distance, ∂V is the surface bounding the volume V that is occupied by the sample, and $\hat{\mathbf{n}}$ is the unit outward normal to this surface at the point $\mathbf{r} \in \partial V$.

For an arbitrary source function we can express the solutions to Eqs. (1) and (2) as

$$u_e(\mathbf{r}) = \int_V G(\mathbf{r},\mathbf{r}')S(\mathbf{r}')\mathrm{d}^3r', \tag{3}$$

$$u_f(\mathbf{r}) = \int_V G(\mathbf{r},\mathbf{r}')a(\mathbf{r}')u_e(\mathbf{r}')\mathrm{d}^3r', \tag{4}$$

where the Green's function $G(\mathbf{r},\mathbf{r}')$ satisfies $[\nabla_{\mathbf{r}}^2 - k^2]G(\mathbf{r},\mathbf{r}') = -(1/D)\delta(\mathbf{r}-\mathbf{r}')$ and $k=\sqrt{\alpha/D}$. In the slab geometry, $G(\mathbf{r},\mathbf{r}')$ is known analytically [9].

In radiative transport theory light propagating through the medium is described by the specific intensity $I(\mathbf{r},\hat{\mathbf{s}})$ at the point $\mathbf{r}$ flowing in the direction of the unit vector $\hat{\mathbf{s}}$. In the diffusion approximation the specific intensity is expanded as $I(\mathbf{r},\hat{\mathbf{s}}) = (c/4\pi)[u(\mathbf{r}) - l^*\hat{\mathbf{s}}\cdot\nabla u(\mathbf{r})]$, where $u(\mathbf{r})$ satisfies one of the diffusion equations (1) and (2) (at the appropriate wavelength) and $l^* = 1/\mu^* = 1/(\mu_a + \mu_s')$ is the transport mean-free-path. In our experiment the measured quantity is the specific intensity that exits the slab in the normal direction. Therefore, we can substitute in the above formula $\hat{\mathbf{s}} = \hat{\mathbf{n}}$, where $\hat{\mathbf{n}}$ is the same outward unit normal that appears in the boundary condition. We then use the latter to express the derivative of $\hat{\mathbf{n}}\cdot\nabla u_f(\mathbf{r})$ at the point $\mathbf{r} = \mathbf{r}_d \in \partial V$ in terms of $u_f(\mathbf{r})$ and obtain

$$I_f(\mathbf{r}_d) = C_d(\mathbf{r}_d)\frac{c}{4\pi}\left(1+\frac{l^*}{l}\right)\int G(\mathbf{r}_d,\mathbf{r})a(\mathbf{r})u_e(\mathbf{r})\mathrm{d}^3r', \tag{5}$$

where we have introduced a phenomenological coupling constant $C_d(\mathbf{r}_s)$, which accounts for the surface area that is mapped onto a given CCD pixel and various imperfections of the optical system.

If a narrow beam is incident on a slab of highly scattering medium in the direction normal to the slab surface (in the positive direction of the z axis), we have [9] $S(\mathbf{r}) = S_0\mu_s' e^{-\mu^*|z-z_s|}\delta(x-x_s)\delta(y-y_s)$. Here S_0 is a constant and $\mathbf{r}_s = (x_s, y_s, z_s)$ is the point at which the incident beam intersects the sample surface. Using this source function, the boundary condition, and the inequality $\mu^* \gg k$ we can evaluate approximately the integral in Eq. (3) to obtain [9] $u_e(\mathbf{r}) = C_s(\mathbf{r}_s)S_0(\mu_s'/\mu^*)(1+l^*/l)G(\mathbf{r},\mathbf{r}_s)$, where $C_s(\mathbf{r}_s)$ is another phenomenological coupling constant. We now combine this equation with Eq. (5) to obtain

$$I_f(\mathbf{r}_d,\mathbf{r}_s) = C_d(\mathbf{r}_d)C_s(\mathbf{r}_s)\frac{cS_0\mu_s'}{4\pi\mu^*}\left(1+\frac{l^*}{l}\right)^2 \times \int_V G(\mathbf{r}_d,\mathbf{r})a(\mathbf{r})G(\mathbf{r},\mathbf{r}_s)\mathrm{d}^3r. \tag{6}$$

Here $I_f(\mathbf{r}_d,\mathbf{r}_s)$ is the intensity measured at the fluorescent wavelength λ_f, which exits the slab at the point $\mathbf{r}_d$ owing to a source beam entering the slab through the opposite face at the point $\mathbf{r}_s$.

The unknown coupling constants $C_d(\mathbf{r}_d)$ and $C_s(\mathbf{r}_d)$ can be eliminated by normalizing Eq. (6) to the intensity $I_e(\mathbf{r}_d,\mathbf{r}_s)$, which is measured at the excitation wavelength. Indeed, arguments similar to those given above lead to the expression $I_e(\mathbf{r}_d,\mathbf{r}_s) = C_d(\mathbf{r}_d)C_s(\mathbf{r}_s)(cS_0\mu_s'/4\pi\mu^*)(1+l^*/l)^2G(\mathbf{r}_d,\mathbf{r}_s)$. We then define the *data function* $\phi(\mathbf{r}_d,\mathbf{r}_s)$ as

$$\phi(\mathbf{r}_d,\mathbf{r}_s) = DG(\mathbf{r}_d,\mathbf{r}_s)\frac{I_f(\mathbf{r}_d,\mathbf{r}_s)}{I_e(\mathbf{r}_d,\mathbf{r}_s)}. \tag{7}$$

In the above formula $I_f(\mathbf{r}_d,\mathbf{r}_s)$ and $I_e(\mathbf{r}_d,\mathbf{r}_s)$ are measured experimentally, while $DG(\mathbf{r}_d,\mathbf{r}_s)$ is known analytically. We have defined the data function in this particular form because the dimensionless variation of the absorption coefficient, $a(\mathbf{r})/\alpha$, is related to ϕ by the following linear integral equation:

$$k^2\int_V DG(\mathbf{r}_d,\mathbf{r})\frac{a(\mathbf{r})}{\alpha}DG(\mathbf{r},\mathbf{r}_s)\mathrm{d}^3r = \phi(\mathbf{r}_d,\mathbf{r}_s). \tag{8}$$

This equation follows directly from Eqs. (1) and (2) without additional approximations. The left-hand side of Eq. (8) is linear in the unknown function $a(\mathbf{r})$, because in writing Eqs. (1) and (2) we have assumed that $\alpha \gg a(\mathbf{r})$. This condition has allowed us to replace the total absorption coefficient in the left-hand sides of these equations by the intrinsic absorption coefficient α. Moreover, Eq. (8) is independent of the unknown coupling coefficients C_d and C_s.

We now notice that Eq. (8) has exactly the same functional form as the integral equation of linearized nonfluorescent OT that was inverted in [3,9,10]. We, therefore, can apply the image reconstruction algorithm developed in these references to invert Eq. (8) and find the function $a(\mathbf{r})$ given a set of measurements of $\phi(\mathbf{r}_d,\mathbf{r}_s)$. Note that the functions $DG(\mathbf{r}_d,\mathbf{r}_s)$ in Eq. (7) and $DG(\mathbf{r}_d,\mathbf{r})$, $DG(\mathbf{r},\mathbf{r}_s)$ depend analytically on the two parameters $k=\sqrt{\alpha/D}$ and l (but not separately on D).

Our experimental setup is described in detail elsewhere [3]. The sample chamber we have used is a rectangular box of a depth of 5 cm with square faces of an area of 50 cm × 50 cm constructed of clear acrylic sheets. The beam is scanned on one face of the sample, and the opposite face is imaged by the CCD and a lens. The chamber is placed equidistantly from the CCD and the laser source along the optical axis at a distance of 110 cm and filled with a scattering medium that consists of a suspension of 1% Intralipid in water. By numerically fitting [12] the Fourier transform of $I_e(\mathbf{r}_d,\mathbf{r}_s)$ with respect to the transverse coordinate of the detector to an analytical formula given in [9], we have found that, for this medium, $k = 0.54\ \mathrm{cm}^{-1}$ and $l = 0.9$ cm. In each experiment, we acquired a data set of $\approx 1.5\times 10^8$ source–detector pairs as described in detail in [3]. The fluorescence was recorded after passing through a narrow bandpass filter (central wavelength 830 nm), which is placed in front of the CCD camera lens.

We inserted two clear glass tubes (inner diameter 16.5 mm, outer diameter 19 mm, axis-to-axis separation 69 mm) into the chamber so that the tube axes were parallel, vertically aligned, and equidistant from the slab surfaces. The tubes contained the same Intralipid solution as the surrounding medium but,

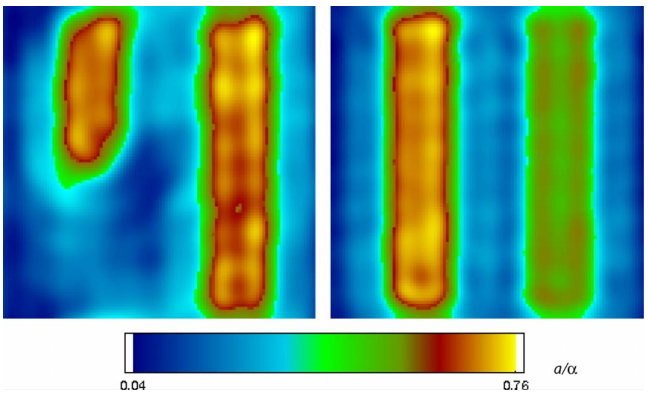

Fig. 1. (Color online) Reconstruction of $a(\mathbf{r})$ for two cylinders filled with an Intralipid solution identical to the surrounding fluid but containing variable amounts of ICG. The field of view is 15 cm × 15 cm. (left) The ICG concentration is 1 mg/L in both tubes, but the left tube is immersed only halfway (with respect to the field of view). (right) Both tubes are immersed all the way but have different ICG concentration: 1 mg/L in the left tube and 2 mg/L in the right tube.

in addition, varying concentrations of ICG. The reconstruction was carried out by inverting Eq. (8). The result (reconstruction of the cross section of the tubes in the central slice) is shown in Fig. 1. Two reconstructions have been made: In the first case, the tubes have the same ICG concentration (1 mg/L) but one of the tubes is inserted only halfway. In the second case, both tubes are fully inserted, but the second tube has a higher ICG concentration (2 mg/L).

As can be seen, the shapes of the cylinders are well reconstructed. We have found that the reconstructed distance between the cylinders's axes is about 68 mm, which is within 1 mm of the independently measured distance of 69 mm. The reconstructed diameters of the cylinders are, however, overestimated: the obtained values are 30 mm for the concentration of 1 mg/L and 40 mm for 2 mg/L. We believe that this overestimation is explained by the ill-posedness of the inverse problem of FOT. Thus, overestimation is stronger for the ICG concentration of 2 mg/L when the signal-to-noise ratio is larger, and the ill-posedness is expected to have a stronger effect.

It can be seen from Fig. 1 (right panel) that the reconstructed ICG concentration depends nonlinearly on the actual concentration. Thus, the image of the tube with 2 mg/L of ICG is weaker than the image of the tube with 1 mg/L of ICG. This is explained by the onset of fluorescence quenching, which takes place at sufficiently high ICG concentrations. In our experiment the measured fluorescent intensity was maximum at the ICG concentration of about 1 mg/L (for ICG dissolved in a 1% Intralipid solution inside the tubes; data not shown). A linear proportionality of the reconstructed and the actual concentrations can be expected at smaller ICG concentrations, as was indeed experimentally observed [6]. Note that the linearity can be expected to extend to substantially larger ICG concentrations if ICG is dissolved in human blood rather than in water [13]. In this reference the maximum of fluorescence intensity was observed at an ICG concentration of 80 mg/L. The explanation of this effect, given in [13], is that in the case of the water solvent ICG molecules form aggregates, which results in a significant decrease of the fluorescence quantum yield. However, in the case of blood, aggregation is inhibited by binding of the ICG molecules to plasma proteins up to much higher ICG concentrations.

In summary, we have demonstrated for the first time reconstruction of a fluorescent agent concentration in a highly scattering medium using a noncontact OT device and data sets in excess of 10^8 independent measurements. We have demonstrated that the fast image reconstruction algorithms developed by us earlier for nonfluorescent OT modalities are fully adaptable to FOT.

This research was supported by the National Institutes of Health (NIH) under grants R21EB004524, R01-EB-002109, and RR-02305.

References and Notes

1. S. R. Arridge, Inverse Probl. **15**, R41 (1999).
2. D. A. Boas, D. H. Brooks, E. L. Miller, C. A. DiMarzio, M. Kilmer, R. J. Gaudette, and Q. Zhang, IEEE Signal Process. Mag. **18**, 57 (2001).
3. Z.-M. Wang, G. Y. Panasyuk, V. A. Markel, and J. C. Schotland, Opt. Lett. **30**, 3338 (2005).
4. G. Turner, G. Zacharakis, A. Soubret, J. Ripoll, and V. Ntziachristos, Opt. Lett. **30**, 409 (2005).
5. Y. Chen, G. Zheng, Z. H. Zhang, D. Blessington, M. Zhang, H. Li, Q. Liu, L. Zhou, X. Intes, S. Achilefu, and B. Chance, Opt. Lett. **28**, 2070 (2003).
6. S. Patwardham, S. Bloch, S. Achilefu, and J. Culver, Opt. Express **13**, 2564 (2005).
7. A. Joshi, W. Bangerth, and E. M. Sevick-Muraca, Opt. Express **14**, 6516 (2006).
8. A. Corlu, R. Choe, T. Durduran, M. A. Rosen, M. Schweiger, S. R. Arridge, M. D. Schnall, and A. G. Yodh, Opt. Express **15**, 6696 (2007).
9. V. A. Markel and J. C. Schotland, Phys. Rev. E **70**, 056616 (2004).
10. V. A. Markel and J. C. Schotland, Appl. Phys. Lett. **81**, 1180 (2002).
11. J. C. Schotland, J. Opt. Soc. Am. A **14**, 275 (1997).
12. We have utilized the nonlinear optimization procedure implemented in GNUPLOT. The two-dimensional spatial Fourier transform of the intensity transmitted through a homogeneous slab was fitted to the analytical formula. Depending on the initial guess, the optimization yielded two distinct sets of parameters: k, l, one of which was used in the image reconstruction, while the other was clearly unphysical ($l > 10$ cm and $k < 0.02$ cm^{-1}) and, therefore, disregarded.
13. R. C. Benson and H. A. Kues, Phys. Med. Biol. **23**, 159 (1978).